Synthesis and characterization of mixed phase anatase TiO$_2$ and sodium-doped TiO$_2$(B) thin films by low pressure chemical vapour deposition (LPCVD)

Yothin Chimupala,*[a] Geoffrey Hyett,[b] Robert Simpson,[a] Robert Mitchell,[c] Richard Douthwaite,[c] Steven J.Milne,[a] and Richard D. Brydson [a]

[a]*Institute of Materials Research, SPEME, University of Leeds, Leeds, LS2 9JT, UK* *Email: pmyc@leeds.ac.uk*
[b]*Department of Chemistry, University of Southampton, Highfield, Southampton, SO17 1BJ, UK*
[c]*Department of Chemistry, University of York, York, YO10 5DD, UK*

TiO$_2$ thin films were synthesized using Low Pressure Chemical Vapour Deposition (LPCVD) onto glass substrates. Titanium isopropoxide (TTIP) and N$_2$ gas were used as the precursor and carrier gas respectively. The effects of reaction temperature, carrier gas flow rate and deposited area were studied. SEM, TEM, powder XRD and UV-Vis and Raman spectroscopy were employed to characterize the phase and morphology of the synthesized materials. The results show that a dual phase (sodium-doped TiO$_2$(B) and anatase) nanocrystalline thin film was successfully prepared by LPCVD with needle- and polygonal plate-shape crystallites respectively. At the interface with the substrate, the thin film deposit exhibited a preferred orientation of TiO$_2$(B) needles in the [001] direction of average crystallite size 50-80 nm in length and 5-10 nm in width, whilst the crystallite size of anatase polygonal-plates was around 200 nm. The optimal LPCVD condition for preparing this mixed phase of TiO$_2$ was 550°C (actual temperature) with a 1 mL/s N$_2$ flow rate. A possible mechanism for the mixed-phase formation by LPCVD on the glass substrates is described as well as the implications for the production of self-cleaning structures.

Introduction

TiO$_2$ semiconductor polymorphs (and in some cases polymorph mixtures) are amongst the most widely used materials owing to their cost effective, highly stable and environmentally-friendly nature combined with their well-known electronic and optical properties.[1] Titania is extensively used for optical applications: as a ubiquitous white pigment, as an opacifier and as an optically reflective coating; additionally it is increasingly used in sunscreens as an ultraviolet (*uv*) blocking agent.[2] Electronically, nanocrystalline and porous titania films are used in the anodes of dye-sensitised solar cells.[3] A further interesting property of titania is the ability to photocatalyse chemical reactions under *uv* irradiation. There are many physical forms of TiO$_2$ photocatalysts including powders, thin films and aqueous suspensions, which have been widely utilized in areas ranging from: treatment of both water and air pollution,[4] water splitting reactions,[5] antibacterial surfaces, through to anti-fogging materials and self-cleaning materials such as window glass.[6,7] A major factor in the practical application of TiO$_2$ photocatalysts, is their ability to be reused whilst retaining high photocatalytic efficiency. In this respect immobilized TiO$_2$ thin films on rigid substrates are a key form if these photocatalysts are to be employed in the various chemical industries and in construction materials.

In the case of self-cleaning materials, TiO$_2$ thin films have been prepared by a wide range of deposition methods such as sol-gel,[8] sputtering,[9] pulsed laser deposition (PLD),[10] physical vapour deposition (PVD)[11] and chemical vapour deposition (CVD)[12]. CVD is a low-cost process, which is easy to set up and subsequently adjust; it permits a high degree of compatibility with a wide range of substrates and also has the potential for mass production. High quality self-cleaning thin films on glass require three major attributes: little or no scattering of visible light, the thin film to be of nanometre dimension in both thickness and crystallite/particle size; a high mechanical resistance to any external abrasion; and finally acceptable photo-catalytic properties such as catalytic-rate and efficiency [6]

Thin films based on the crystalline anatase phase of TiO$_2$ are used in self-cleaning glass/windows[6] as this polymorph possesses a higher photocatalytic activity than rutile. For industrial production, the thin films are exclusively the anatase phase, 50-500 nm thick and deposited using atmospheric pressure CVD from TiCl$_4$ and ethyl acetate precursors at temperatures between 400-660 ^{o}C.[13] Current improvement strategies focus on the use of ultrafine nanoparticles in the thin films, the modification of charge transfer processes to prevent the recombination reaction, and the controlled production of phase mixtures in the thin films which may provide higher photocatalytic activities. Mixing two different phases of TiO$_2$ (ref. 14 and 15) such as anatase/rutile or anatase/TiO$_2$(B), directly affects the charge transfer process between the different phases possibly reducing recombination of photo-generated

electrons and so enhancing the photocatalytic activity.[16–19] This directly improves the efficiency of oxidative stripping of organic molecules from water or air.

The $TiO_2(B)$ or bronze phase of titania has attracted significant interest over the last decade because of the distinctive monoclinic crystal structure which, because of its low-density crystal framework, exhibits larger channels and voids and also a higher specific storage capacity as compared to the tetragonal structures of anatase and rutile[20–22] as shown in Fig 1. Commonly, alkali metal titanates have been used as precursors for $TiO_2(B)$ preparation in many synthetic methods such as sol-gel,[23] hydrothermal[24] and solid-state reaction.[21] In this paper, the LPCVD method was employed to synthesise (for the first time) dual phase anatase and sodium-doped $TiO_2(B)$ thin films on glass substrates.

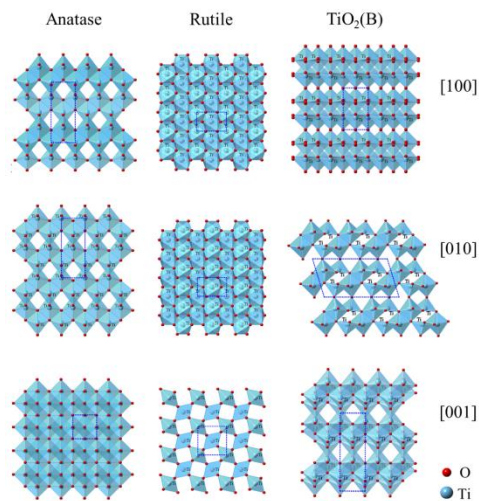**Fig.1** Crystal structures of anatase, rutile and $TiO_2(B)$ viewed along a, b and c axes.

Experimental Procedure

Thin Film Preparation

Low pressure chemical vapour deposition (i.e. thermal decomposition and oxidation of a precursor) at 25 mbar was used to synthesize TiO_2 thin films on substrates as shown schematically in Fig. 2. Titanium tetra-isopropoxide (TTIP, 97%) was used as the titania precursor, 5-10 mL being placed in a bubbling chamber which was set in an oil bath at 90°C. The reactor was a quartz cylinder tube placed in a tube furnace and was pre-heated from room temperature up to the desired reaction temperature. N_2 gas with a flow rate of 1 L/min was used to carry the TTIP vapour into the reactor. Titania thin films were deposited onto different substrates including: a soda-lime glass slide (with wt% composition of 72.00 SiO_2, 14.50 Na_2O, 7.05 CaO, 3.95 MgO, 1.65 Al_2O_3, 0.30 K_2O and 0.06 Fe_2O_3) of dimensions 12 mm × 152 mm × 1 mm (width × length × thickness) and fused quartz (pure amorphous silica of the same dimensions). The reaction temperature in the tube furnace was varied between 450 and 600°C with a reaction time of typically 15 min. However, we note that this is only a nominal temperature as there will exist a temperature gradient inside the reaction tube. This temperature gradient was measured in air as a function of position inside the reaction tube using a moveable thermocouple and the results for a nominal furnace temperature of 600 °C are shown in Fig. 2b.

Materials Characterization

Before being characterized, the TiO_2 film deposited onto the substrate (e.g. a soda-lime glass slide) was divided into 12 plates each of dimensions 12 mm × 12.6 mm × 1 mm. These samples represented different reactor positions relative to the gas entry point at plate1. In-plane and out of plane X-ray diffraction (XRD) with a Philips X'Pert MPD diffractometer using Cu K_α X-ray radiation, were employed to characterise the crystalline phases in the samples. The surface morphology and thickness of TiO_2 thin films were investigated by scanning electron microscopy (SEM, Carl Zeiss LEO 1530 Gemini FEGSEM) and energy dispersive X-ray (EDX) spectroscopy (Oxford Instruments) both in plan-view and in cross-section. Raman spectroscopy (Renishaw's inVia Raman microscope with green laser of wavelength 514.5 nm^{-1}) and UV-Vis diffuse reflectance spectroscopy (Perkin Elmer UV-vis Lambda 900) were also used to characterise these materials. Initial sample preparation for transmission electron microscopy (TEM) was achieved by using a scalpel to scrape off the deposited materials from the substrates onto a holey carbon film supported on a Cu TEM grid. In addition a Focused Ion Beam (FIB − FEI Nova

200) was used to prepare thin cross-sections of these materials on the substrates for TEM analysis using imaging, selected area electron diffraction (SAED) and EDX spectroscopy, mapping and quantification (Oxford Instruments AZTEC) on a FEI Tecnai G2 TEM/STEM operated at 200 kV.
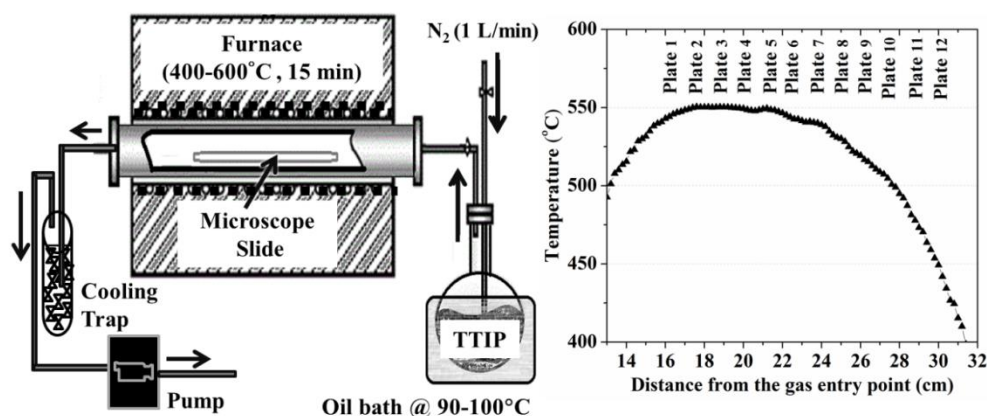

Fig.2 (a) Schematic representation showing the LPCVD system for preparing TiO_2 (b) Temperature profile in the tube furnace for a nominal reaction temperature of 600°C.

Results

The optimum synthesis condition to achieve thin films composed of mixed phase $TiO_2(B)$ and anatase was found to be a nominal reaction temperature of 600°C for 15 min reaction time with 5 mL of TTIP. The mixed phase of TiO_2 only occurred when the nominal reaction temperature reached $600^{\circ}C$. At lower nominal temperatures such as 400°C and $500^{\circ}C$, thin films tended to be composed of pure anatase with an equiaxed particle morphology exhibiting extensive particle aggregation, whilst at high temperatures (700°C) it was observed that the substrate began to deform and the deposit consisted of pure anatase with a non-aggregated spherical particle morphology. In this report we focus solely on the results obtained at a nominal temperature of 600°C as these conditions appear to promote the formation of the $TiO_2(B)$ phase. As shown in Fig. 2b the actual temperature in the reaction tube had a maximum of *ca.* 550°C at the position of plates 2-5 and decreased towards each end of the tube.
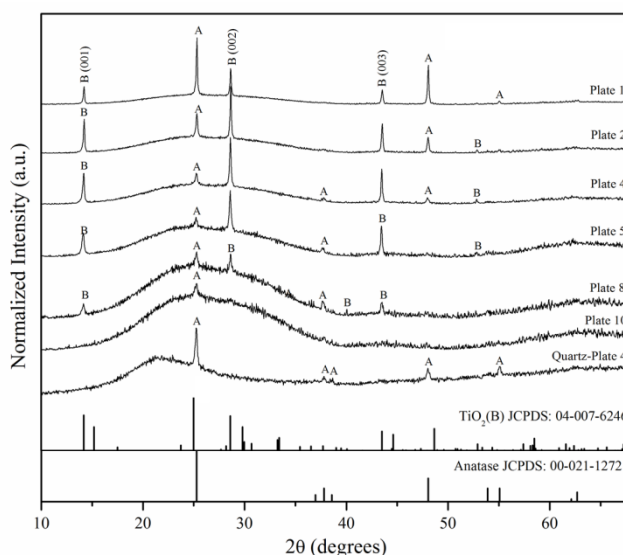

Fig. 3 Out of plane XRD patterns of TiO_2 thin film deposited onto soda-lime glass substrates and a quartz substrate at position Plate 4 prepared by LPCVD at 600°C: A and B refer to the assignment of the anatase and $TiO_2(B)$ phases respectively.

For these conditions, the out of plane XRD patterns of a selection of 12 plates on a soda-lime glass substrate are shown in Fig. 3, and are compared to the corresponding thin film on a fused quartz substrate (referred to as TiO_2-Quartz) prepared under identical conditions and reactor position as Plate 4. The XRD patterns show that almost all of 600°C synthesized thin films on soda lime glass substrate consist of a combination of both $TiO_2(B)$ (JCPDS 04-007-6246) and anatase phases (JCPDS 00-021-1272) in different relative proportions depending on the distance from the gas entry point. As will become clear later, it is important to note that the XRD peaks assigned to the $TiO_2(B)$ phase do not match with any sodium titanate

$Na_xTiO_{2+0.5X}$ phase or any other related sodium-containing phase in the JCPDS database. In Plate 1 anatase is the majority component, nevertheless in other reactor positions (as shown in Plates 2, 4, 5 and 8) XRD indicates the main component is the TiO_2(B) phase. In the case of Plate 10, the patterns show only one peak at $2\theta = 25.30°$ indicating the anatase phase and two very broad features lying between 15-35° and 60-70° characteristic of amorphous SiO_2 from the glass substrates. The influence of the substrate was more evident at larger distances from the gas entry point possibly indicating the presence of a thinner crystalline deposit.

The influence of the substrate on the film was studied using a fused-quartz plate (at the same position as Plate 4) instead of the normal soda-lime glass substrate under the same synthesis conditions. The differences can be seen in Fig. 3 by comparing the XRD patterns labeled Plate 4 and Quartz-plate 4 respectively. These results indicate that a mixed phase of anatase and TiO_2(B) can be indexed on Plate 4, whilst only the anatase phase is evident on a fused quartz substrate indicating that the soda-lime glass substrate promotes the formation of TiO_2(B) by LPCVD.

The (101) and (200) peaks of the anatase phase (at $2\theta = 25.28°$ and 48.05° respectively) are very close to the (110) and (020) peaks of the TiO_2(B) phase at $2\theta=24.98°$ and 48.63°. The crystallite size derived from XRD line broadening in Fig. 3 was estimated to be in the range 40-60 nm for both phases. In order to clarify the results, both in-plane and out-of-plane XRD were recorded for Plate 4 to confirm the existence of both phases, as illustrated in Fig. 4. The in-plane XRD pattern shows additional peaks of the TiO_2(B) phase when compared to the TiO_2(B) peaks evident in the out-of-plane pattern. Not only does this confirm the existence of the TiO_2(B) phase it also reveals a preferred [001] crystallographic orientation of TiO_2(B) as illustrated by the strong (001), (002) and (003) hkl reflections at $2\theta = 14.16°$, 28.62° and 43.5° in the out-of-plane pattern.

Raman spectroscopy was employed to confirm the phases on Plate 4 and Quartz-plate 4. The Raman active modes for anatase are evident as an intense peak around 144 cm^{-1} as well as three other peaks at 395, 517 and 637 cm^{-1} present in both samples and indicating solely pure anatase on Quartz-plate 4 (Fig. 5). The remaining peaks, especially two strong peaks at 121.9 and 144.96 cm^{-1} signify the Raman active modes of the TiO_2(B) phase[25,26] indicating the presence of the mixed phase on Plate 4.
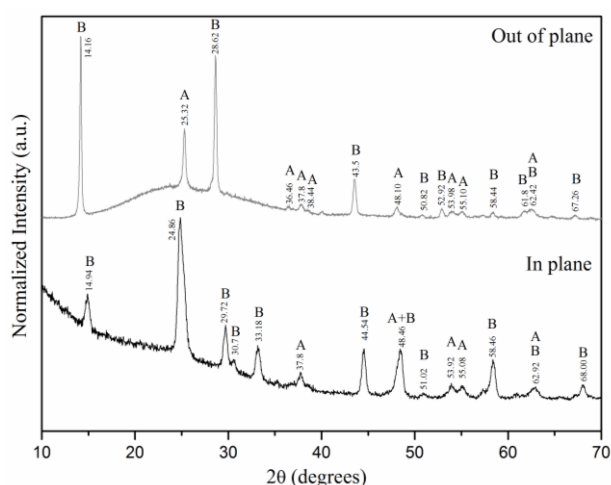

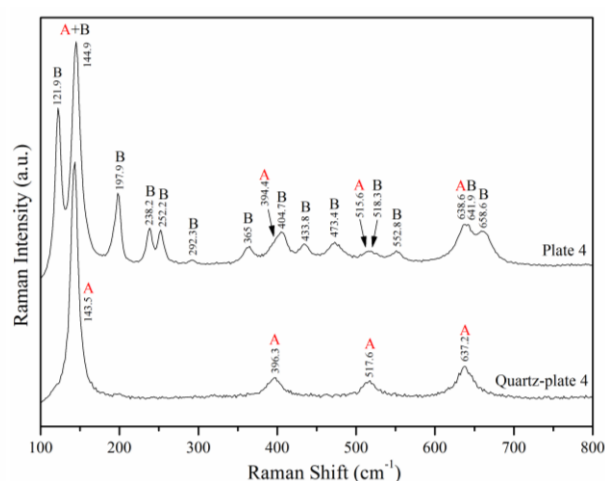**Fig 4.** In plane and out of plane XRD patterns of Plate 4: A and B refer to anatase and TiO_2(B) phases respectively.

Fig 5. Raman spectra of Plate 4 and Quartz-plate 4: A and B indicate the anatase and TiO_2(B) phases respectively.

UV-Vis diffuse reflectance spectroscopy was used to study optical properties of the thin films and raw spectra are shown in Fig. 6(a)[16] and the same data after a transformation to absorption in Fig. 6(b). The band gaps of these materials were calculated by extrapolating the linear portion of the slopes in Fig. 6(b) and determining the intercept with the background. The band gap energies of anatase and TiO_2(B) are experimentally reported as being 3.2 eV and 3.0-3.2 eV respectively[26–30]. The present results curiously show a energy band gap of between 3.25 and 3.31 eV which increased with an increasing proportion of the TiO_2(B) phase. It might be expected that the presence of any dopants in the thin film may cause changes including possible increases in the band gap energy. In contrast, the anatase thin film on Quartz-plate 4 showed a band gap of 3.275 eV.
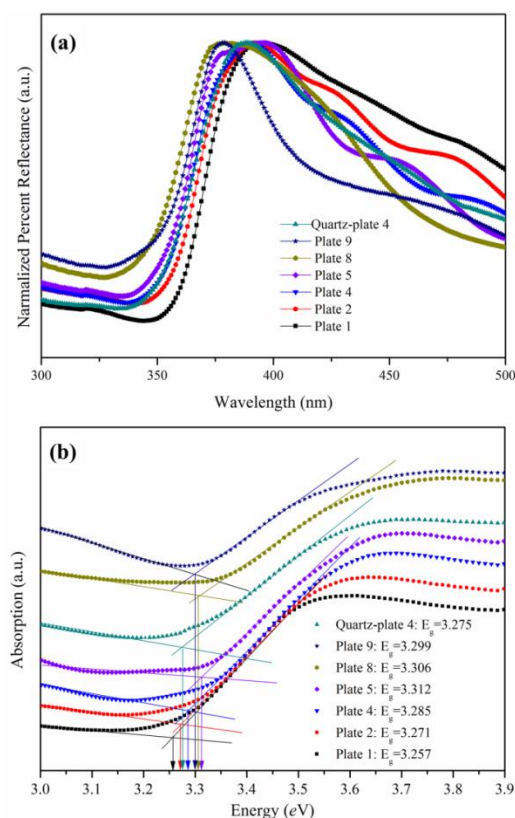
Fig 6. (a) UV-Vis diffuse reflectance spectrums of the samples prepared at optimum condition (b) Estimation of the band gap energy by plotting the corresponding graph of absorption versus photon energy (*e*V).

A SEM plan-view image of Plate 4 is shown in Fig. 7a and illustrates the presence of two types of particle morphology: large polygonal plates 100-200 nm in diameter and smaller, more spherical particles with a diameter of around 20 nm. The average primary particle size of this bimodal distribution at the film surface is 73±42 nm. A composition derived from SEM/EDX, shown inset in Fig. 7a, confirms the existence of titanium and oxygen in the thin film. As the TiO_2 film thickness is only around -200 nm, as shown in the SEM cross-section in Fig. 8a, the electron beam interaction volume also samples the glass substrate and hence the Ti:O ratio is less than 1:2 and this is also presumably why Na, Si, Ca and Mg are detected. Inspection of Fig. 8a, reveals that the film cross-section also contains two kinds of particles: smaller columnar or needle-shaped particles present predominantly at the glass substrate/film boundary and the larger plate-like particles predominantly deposited on the film surface. This may suggest that the small needle-shaped particles are acting as a seeding layer on the substrate or arise from some sort of interfacial reaction with the substrate. As shown in the graph in Fig. 8c and in the images in Fig. 8d, the film thickness decreases from 400 to 50 nm dependent on the distance from the carrier gas entry point, most likely due to precursor depletion. Thus both the thickness and the relative proportion of the different crystalline phases are directly dependent on the position of the substrate in the reactor. Interestingly from the plan-view image of the Quartz-plate 4 sample shown in Fig. 7b, the pure anatase particles so produced exhibit a size of 30 nm and a different spherical morphology, similar to anatase samples synthesized at reaction temperatures below 500°C and above 700°C on soda-lime glass substrates. A SEM cross section image of Quartz-plate 4 (Fig. 8b) shows a unique columnar morphology across the thin film with no apparent phase at the film-substrate interface.
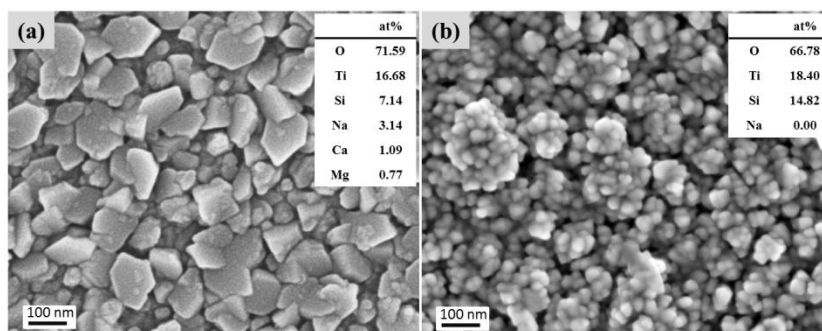

Fig 7. (a) SEM secondary electron image of TiO_2 thin film from the top surface of Plate 4; (b) SEM secondary electron image of TiO_2 thin film from the top surface of Quartz-plate 4
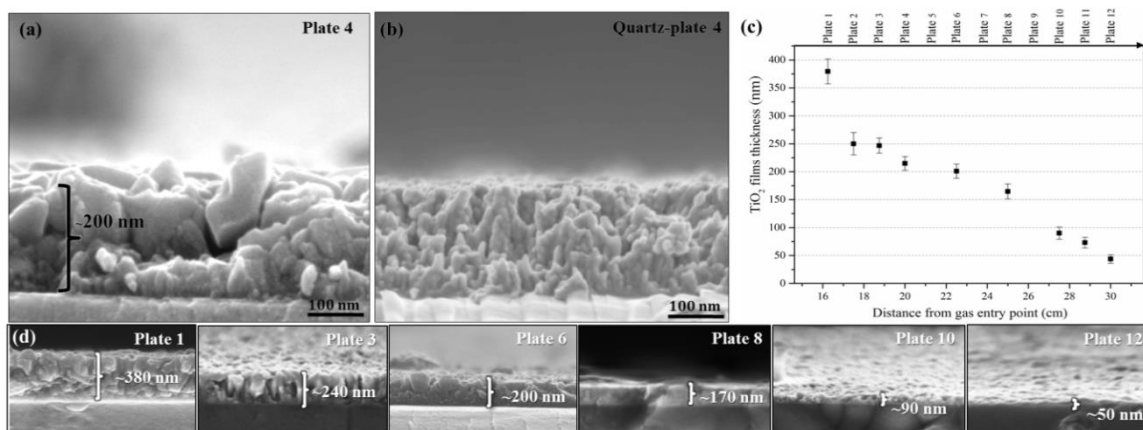
Fig 8. SEM cross-sectional images of thin film fracture surfaces of Plate 4 on: (a) soda lime glass and (b) fused quartz substrates; (c) Plot of the film thickness relative to the gas entry point observed from SEM cross-sectional images of thin films on soda lime glass substrates shown in Fig. 8d: (d) The decreasing of TiO_2 film thickness on Soda lime glass substrate relative to the gas entry point.
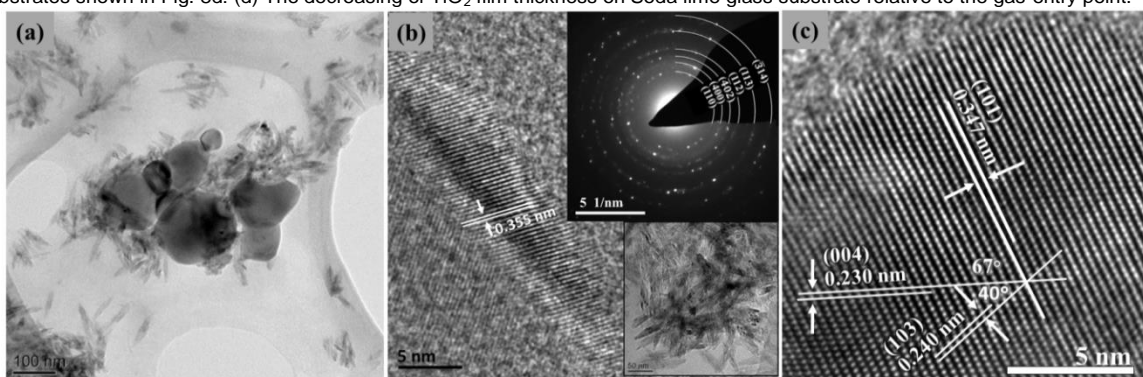

Fig 9. (a) A TEM image taken from Plate 4, showing both anatase polygonal plates and TiO_2(B) needle-shaped particles; (b) HRTEM and diffraction pattern of a TiO_2(B) needle; (c) HRTEM image of an anatase polygonal plate.

The coexistence of TiO_2(B) and anatase phases in the thin films confirmed by XRD and Raman results may explain the two types of particle morphology observed in SEM images. These two distinct types of particle morphology (small needle-shaped and larger polygonal plate-like) are also evident in TEM of thin film material scraped from the surface of Plate 4, a typical TEM image being shown in Fig. 9a. The particle size of the polygonal plates are in the range 40-220 nm with an average of around 150 nm, significantly bigger than the needles which are in the range 5-10 nm in width and 50-80 nm in length. These values are consistent with the XRD results on the assumption that the short axis of the polygonal plates lies parallel to the substrate. HRTEM and SAED were employed to investigate the relationship between physical appearance and the nanostructure of these morphologies as illustrated in Fig. 9b and 9c. In Fig. 9b, the needle-like crystals clearly show a lattice spacing of 3.55Å which can be tentatively assigned to the (110) lattice spacing of TiO_2(B). Moreover, a TEM selected area diffraction pattern of a group of needles, shown inset in Fig. 9b, shows rings corresponding to the (110), (400), ($\bar{4}$02), (112), (113) and ($\bar{3}$14) spacings of TiO_2(B). TEM/EDX spectra (Fig. 10a) of the same area reveals the presence of Ti, O and also a very small amount of Na typically less than 1% atomic, however interference between the Cu L- (from the TEM support grid) and Na K-X-ray emission peaks makes this quantification unreliable. Fig. 9c demonstrates that the polygonal plate is anatase as it reveals lattice spacings of 3.47Å, 2.38Å and 2.28Å which correspond to the (101), (103) and (112) interplanar spacings respectively. TEM/EDX on the anatase plates reveals the presence of solely Ti and O (Na, if present, is below the level of detectability following quantification), as shown in Fig. 10b.
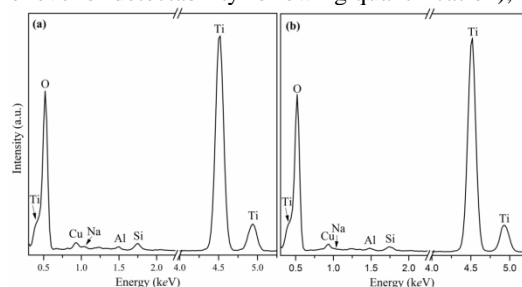

Fig. 10. TEM-EDS spectrum of: (a) a group of needles particles investigated in the same area of fig.9b;(b) a polygonal plate particle correlated with fig.9C

The FIB lift out method was used to prepare a thin cross-sectional TEM sample of Plate 4 as shown in Fig. 11a. HRTEM images are presented from two different areas on this cross section: one in a region near the top surface of thin film (Fig. 11b) showing the lattice spacings of anatase TiO_2; whilst the other is from an area close to the interface between the TiO_2 film and the substrate shown in Fig. 11c. In Fig. 11a (inset) and 11c, a number of needle particles are observed at the interface between the glass substrate and the TiO_2 thin film deposit, these exhibit lattice spacings of 3.59Å and 6.21Å consistent with the (110) and (001) spacings of TiO_2(B) respectively. The majority of needle particles exhibited a preferred growth direction along [001] (as suggested by XRD), however some showed orientations corresponding to [110] and close to [111].

When combined with the XRD results, this suggests that predominantly the needles grow preferentially along their long axis ([001] direction) perpendicular to the substrate, i.e. oriented vertically as illustrated schematically in Fig. 14. Note this is different to the findings of Li et al. (2011) on powders of TiO_2(B) nanowires grown by hydrothermal synthesis who propose a preferred <110> orientation in the nanowires.[31]

Phase-formation in the thin film was investigated by Scanning TEM (STEM) and EDX spectroscopy on the FIB cross-section. STEM/EDX elemental maps, shown in Fig. 12, indicate the presence of relatively high concentrations of Na (typically a Na/Ti elemental ratio of ca. 0.2) at the interface between the glass substrate and the TiO_2 film. STEM/EDX line scans also confirm a concentration gradient of Na presumably arising as a result of diffusion from the glass substrate as shown in Fig. 13 Generally the level of Na gradually decreases with increasing distance from the substrate interface, however there also seems to be a build-up of Na at the top film surface evident in both the maps and the line scans. The present results all indicate that the presence of Na arising from diffusion from the soda lime glass substrate is associated with the formation of a reaction layer of the TiO_2(B) phase at the film/substrate interface. This interfacial layer is absent when the thin film is grown on fused quartz, which does not contain sodium. From the pXRD data it is clear that anatase is present even when TiO_2(B) is absent and thus the TiO_2(B) layer does not appear necessary to seed growth of anatase.
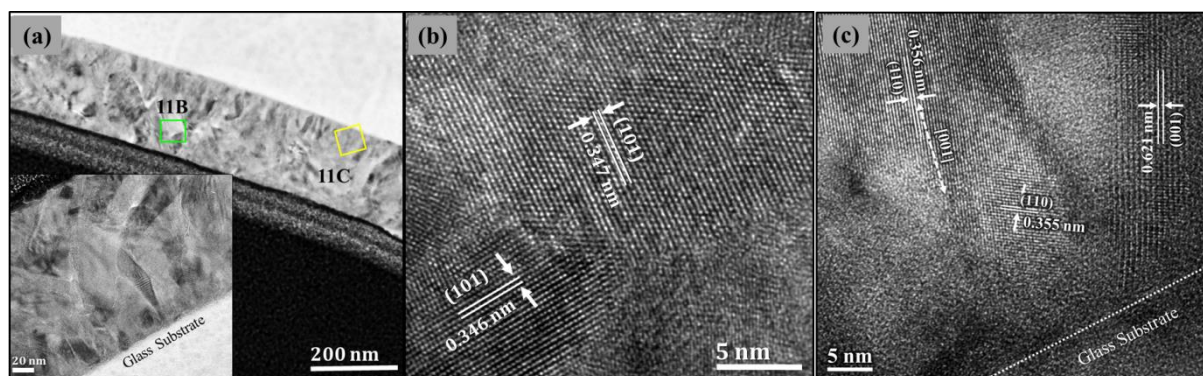

Fig. 11. (a) A TEM image of FIB cross section of Plate 4;(b) A HRTEM image taken from FIB-section at a square area lebeled as 11B on the fig.11(a), showing lattice spaces of anatase polygonal plates; (c) A HRTEM image taken from different square area of the fig.11(a), labeled as 11C of TiO_2(B) needle-shaped particles illustrates (110)and (001) spacings.

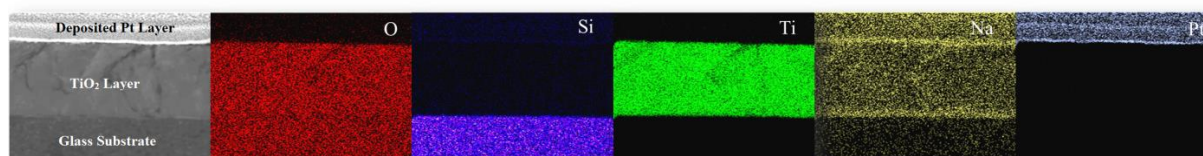**Fig. 12**. STEM-EDS elemental maps of FIB cross section of Plate 4

Discussion

The literature for the preparation of TiO_2(B) has, until now, concentrated exclusively on the production of powders using synthesis routes such as hydrothermal and sol-gel methods and there is no mention of CVD. All these synthesis routes utilise the same key concept, involving the use of NaOH in addition to the main titanium precursor.[32,33] All propose similar steps in the synthesis mechanism involving: (1) incorporation of Na^+ into the TiO_2 crystallite forming Sodium Titanate as a first intermediate material; (2) Na^+ in the Sodium Titanate structure is exchanged with H^+ from an acidic solution during post-synthesis processing, producing a second intermediate phase of Hydrogen Titanate; (3) finally a thermal treatment is used to transform the unstable phase of H_xTiO_y to the more stable phases of TiO_2 depending on the heat treatment temperature.[34]
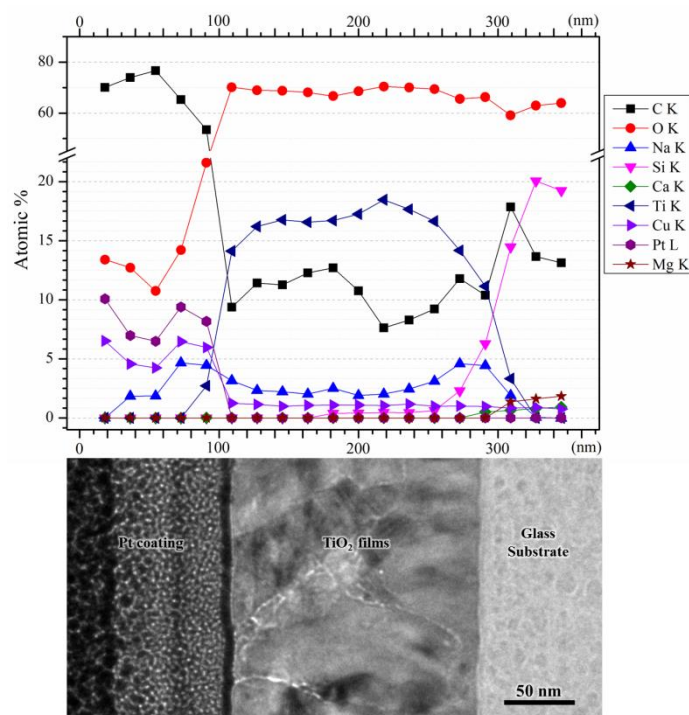
Fig. 13. STEM-EDS line scanning of FIB cross section of Plate 4.

However, NaOH was not used as a precursor during the present LPCVD deposition of the thin films. However Na is a major constituent of soda lime glass and may contain up to 5 atom% Na [6]. The silicon-oxygen tetrahedron is the basic building block of the glass framework however cations such as Na^+ ions usually perform the function of cationic counterparts at non-bridging oxygen units. Thus, the Na^+ ions are considered to be mobile. Diffusion of Na^+ from the glass substrate could occur at deposition temperatures of 600°C which is higher than the range of glass transition temperatures of commercial soda-lime glass slides – usually between 564 to 573°C[35]. We calculate the diffusion coefficient of Na^+ in soda-lime glass at 600°C to be of the order of 4×10^{-7} cm^2/s,[36] furthermore the diffusivity of Na^+ increases as pressure is decreased,[37] which implies that during reaction sodium ions could diffuse hundreds of microns and hence throughout the film.

From these results it can be concluded that LPCVD deposition method at 600°C with a TTIP precursor normally promotes the formation of the TiO_2 anatase phase on a general substrate, however the existence of Na^+ ions which have diffused from a substrate such as a soda lime glass slide encourages the formation of an oriented $TiO_2(B)$ reaction layer during TiO_2 thin film deposition. This potential mechanism for $TiO_2(B)$ formation in the LPCVD process is shown in Fig.14. Here we propose three steps for the $TiO_2(B)$ formation: (1) Na^+ ions migrate to the surface of the substrate during the pre-heat treatment process;[38] (2) owing to higher negative charge of non-bridging oxygen units of TiO_2 than SiO_2, the Na^+ ions prefer to diffuse from the surface of the substrate into the nascent TiO_2 films leaving a Na-depleted zone in the region of glass neighboring the TiO_2 film;[39] (3) a seeding intermediate phase is formed and this decomposes at temperature so forming $TiO_2(B)$ needles and leaving Na^+ ions to continuously migrate to the upper surface of the thin film. Further into the film and in the absence of significant amounts of Na, the titania deposits and forms anatase instead of $TiO_2(B)$ depending on the reaction temperature. This assumption is partially supported by previously reported research where migration from soda glass slide to the initial stages of growth of TiO_2 films produced only brookite TiO_2 or an incomplete phase referred to as $Na_2O.xTiO_2$.[40,41] Finally it has been reported that $TiO_2(B)$ synthesized from sodium-containing starting materials promotes particle needle, tube- and rod-shaped morphologies with a preferred growth direction[16,23,42,43] consistent with the needle-morphologies observed in this research.

A number of research reports have indicated improved efficiencies of mixed-phase anatase and $TiO_2(B)$ over single phase material (either anatase or $TiO_2(B)$) for the case of a number of photocatalyst reactions including: methyl orange degradation,[17] sulforhodamine B degradation,[16] methylene blue degradation,[44] active yellow XRG dye degradation,[45] nitrate reduction[15] and the water splitting reaction.[46] As far as we are aware, there have been no reports of the application of mixed-phase materials in self-cleaning glass, however such materials could in principle lead to improved photocatalytic efficiencies. Furthermore, $TiO_2(B)$ nanocrystalline thin films have been fabricated using spin-dip coating onto conductive glass substrates for use as a replacement for graphite anodes in lithium ion batteries.[22] Potentially the high surface area and mesoporosity of such nanostructured films could lead to improved storage capacities and the present CVD route may offer a potential alternative route for their fabrication provided a sodium source could be incorporated in the substrate.
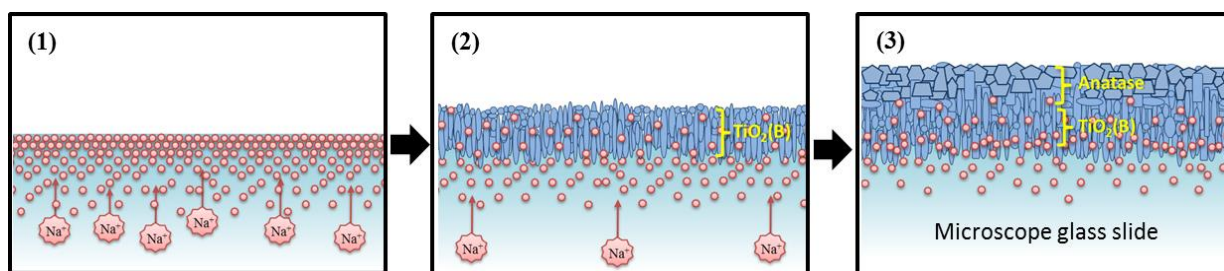
Fig. 14. Proposed mechanism for synthesis of mixed phase TiO$_2$ thin films by LPCVD method

Conclusions

Titania films have been prepared by low pressure chemical vapour deposition on soda-lime glass substrates. Using 5 mL of a TTIP precursor deposited for 15 min at 550°C (actual temperature) on the substrate, around 200 nm thick TiO$_2$ thin films consisting of dual phase monoclinic TiO$_2$(B) needles and larger anatase polygonal plates were observed. The small nano-needles of the TiO$_2$(B) phase were located at the interface with the substrate and exhibited a preferred orientation along [001]. These needles were absent when the substrate was fused quartz. A mechanism for the CVD synthesis of TiO$_2$(B) is presented involving diffusion of Na from the glass substrates. To our knowledge, this is the first time the monoclinic TiO$_2$(B) phase has been prepared by a CVD method. Potentially this fabrication route could be of benefit for production of photocatalytic devices and replacement anodes for lithium ion batteries.

Acknowledgements

Notes and references

1   M. R. Hoffmann, S. T. Martin, W. Choi, and D. W. Bahnemannt, *Chem. Rev.*, 1995, **95**, 69.
2   J. F. Jacobs, I. van de Poel, and P. Osseweijer, *Nanoethics*, 2010, **4**, 103.
3   X. Chen and S. S. Mao, *Chem. Rev.*, 2007, **107**, 2891.
4   T. Kamegawa, N. Suzuki, and H. Yamashita, *Energy Environ. Sci.*, 2011, **4**, 1411.
5   A. Fujishima, T. N. Rao, and D. A. Tryk, *J. Photochem. Photobiol. C Photochem. Rev.*, 2000, **1**, 1.
6   Y. Paz, Z. Luo, L. Rabenberg, and a. Heller, *J. Mater. Res.*, 2011, **10**, 2842.
7   X. Zhao, Q. Zhao, J. Yu, and B. Liu, *J. Non. Cryst. Solids*, 2008, **354**, 1424.
8   A. Bittner, R. Jahn, and P. Löbmann, *J. Sol-Gel Sci. Technol.*, 2011, **58**, 400.
9   P. Löbl, M. Huppertz, and D. Mergel, *Thin Solid Films*, 1994, **251**,72.
10   H. Lin, A. K. Rumaiz, M. Schulz, D. Wang, R. Rock, C. P. Huang, and S. I. Shah, *Mater. Sci. Eng. B*, 2008, **151**, 133.
11   J.-D. Kwon, J.-J. Rha, K.-S. Nam, and J.-S. Park, *Jpn. J. Appl. Phys.*, 2011, **50**, 085502.
12   H. Lee, M. Y. Song, J. Jurng, and Y.-K. Park, *Powder Technol.*, 2011, **214**, 64.
13   S. a. O'Neill, R. J. H. Clark, I. P. Parkin, N. Elliott, and A. Mills, *Chem. Mater.*, 2003, **15**, 46.
14   A. J. Cross, C. W. Dunnill, and I. P. Parkin, *Chem. Vap. Depos.*, 2012, **18**, 133.
15   M. M. Mohamed, B. H. M. Asghar, and H. A. Muathen, *Catal. Commun.*, 2012, **28**, 58.
16   D. Yang, H. Liu, Z. Zheng, Y. Yuan, J. Zhao, E. R. Waclawik, X. Ke, and H. Zhu, *J. Am. Chem. Soc.*, 2009, **131**, 17885.
17   C. Huang, K. Zhu, M. Qi, Y. Zhuang, and C. Cheng, *J. Phys. Chem. Solids*, 2012, **73**, 757.
18   Z. Zheng, H. Liu, J. Ye, J. Zhao, E. R. Waclawik, and H. Zhu, *J. Mol. Catal. A Chem.*, 2010, **316**, 75.
19   Y. Bai, W. Li, C. Liu, Z. Yang, X. Feng, X. Lu, and K.-Y. Chan, *J. Mater. Chem.*, 2009, **19**, 7055.
20   T. P. Feist and peter K. Davies, *J. Solid State Chem.*, 1992, **101**, 275.
21   M. René, B. Luc, and T. Michel, *Mater. Res. Bull.*, 1980, **15**, 1129.
22   A. G. Dylla, P. Xiao, G. Henkelman, and K. J. Stevenson, *J. Phys. Chem. Lett.*, 2012, **3**, 2015.
23   R. Giannuzzi, M. Manca, L. De Marco, M. R. Belviso, A. Cannavale, T. Sibillano, C. Giannini, P. D. Cozzoli, and G. Gigli, *ACS Appl. Mater. Interfaces*, 2014, **6**, 1933.
24   A. R. Armstrong, G. Armstrong, J. Canales, R. García, and P. G. Bruce, *Adv. Mater.*, 2005, **17**, 862.
25   T. Beuvier, M. Richard-plouet, and L. Brohan, *J. Phys. Chem. C*, 2009, **113**, 13703.
26   M. Ben Yahia, F. Lemoigno, T. Beuvier, J.-S. Filhol, M. Richard-Plouet, L. Brohan, and M.-L. Doublet, *J. Chem. Phys.*, 2009, **130**, 204501.
27   X. Wang, G. Wu, B. Zhou, and J. Shen, *Materials*, 2013, **6**, 2819S.
28   F. P. Koffyberg, K. Dwight, and A. Wold, *Solid State Commun.*, 1979, **30**, 433.
29   G. Betz and H. Tributsch, *J. Appl. Electrochem.*, 1984, **14**, 315.
30   G. Nuspl, K. Yoshizawa, and T. Yamabe, *J. Mater. Chem.*, 1997, **7**, 2529.
31   J. Li, W. Wan, H. Zhou, J. Li, and D. Xu, *Chem. Commun. (Camb).*, 2011, **47**, 3439.

32 C.-W. Peng, T.-Y. Ke, L. Brohan, M. Richard-Plouet, J.-C. Huang, E. Puzenat, H.-T. Chiu, and C.-Y. Lee, *Chem. Mater.*, 2008, **20**, 2426.

33 T. Beuvier, M. Richard-Plouet, and L. Brohan, *J. Phys. Chem. C*, 2010, **114**, 7660.

34 V. Gentili, S. Brutti, L. J. Hardwick, A. R. Armstrong, S. Panero, and P. G. Bruce, *Chem. Mater.*, 2012, **24**, 4468.

35 A. Fluegel, D. A. Earl, A. K. Varshneya, and D. Oksoy, in *High Temperature Glass Melt Property Database for Process modeling*, ed. T. P. Seward III and T. Vascott, The American Ceramic Society, Westerville, Ohio, 2005, vol. 1, ch. 9, pp. 187-257.

36 M. Braedt and G. H. Frischat, *Commun. Am. Ceram. Soc.*, 1984, c54.

37 J. G. Bryce, F. J. Spera, and D. J. Stein, *Am. Mineral.*, 1999, **84**, 345.

38 G. H. Frischat, *J. Am. Ceram. Soc.*, 1968, **51**, 528.

39 E. Aubry, J. Lambert, V. Demange, and a. Billard, *Surf. Coatings Technol.*, 2012, **206**, 4999.

40 H. Schroeder, in *Physics of thin films*, ed. G. Hass and R. E. Thun, Academic press, New York and London, 5th edn., 1969, vol. 5, pp. 87–140.

41 C. Ohara, T. Hongo, A. Yamazaki, and T. Nagoya, *Appl. Surf. Sci.*, 2008, **254**, 6619.

42 A.R. Armstrong, G. Armstrong, J. Canales, and P. G. Bruce, *Adv. Mater.*, 2005, **17**, 862.

43 Z. Liu, Y. G. Andreev, A. Robert Armstrong, S. Brutti, Y. Ren, and P. G. Bruce, *Prog. Nat. Sci. Mater. Int.*, 2013, **23**, 235.

44 C.-W. Peng, M. Richard-Plouet, T.-Y. Ke, C.-Y. Lee, H.-T. Chiu, C. Marhic, E. Puzenat, F. Lemoigno, and L. Brohan, *Chem. Mater.*, 2008, **20**, 7228.

45 J. Zhu, J. Zhang, F. Chen, and M. Anpo, *Mater. Lett.*, 2005, **59**, 3378.

46 S. K. Parayil, H. S. Kibombo, L. Mahoney, C. Wu, M. Yoon, and R. T. Koodali, *Mater. Lett.*, 2013, **95**, 175.